Docking Experiment in Dark Environments Using Active/Lighting Marker and HSV Correlation

1st Daiki Yamada
Natural Science and Technology
Okayama University
Okayama, Japan
p7kw2h27@s.okayama-u.ac.jp

2nd Naoki Mukada
Natural Science and Technology
Okayama University
Okayama, Japan
pola9zud@s.okayama-u.ac.jp

3rd Myo Myint
Natural Science and Technology
Okayama University
Okayama, Japan
puqs1ci8@s.okayama-u.ac.jp

4th Khin Nwe Lwin
Natural Science and Technology
Okayama University
Okayama, Japan
pdoj8yez@s.okayama-u.ac.jp

5th Takayuki Matsuno
Natural Science and Technology
Okayama University
Okayama, Japan
matsuno@cc.okayama-u.ac.jp

6th Mamoru Minami
Natural Science and Technology
Okayama University
Okayama, Japan
minami-m@cc.okayama-u.ac.jp

***Abstract*—Recharging ability with underwater docking function would be a first primal step conducted to enable the AUV to operate independently of a surface vessel for extended periods. Therefore, the role of docking operation came in picture not only for battery recharging application but also other novel applications such as sleeping under mother ship, or new mission up and down loading. Moreover, docking capacity can be extended to provide navigation for other underwater vehicles on the way of their mission too. However, there are many challenging issues in achieving these applications that request high accuracy and robustness against disturbances that are provided by the underwater environment. The most challenging and unavoidable problems in sensing sphere for sea operations are, we think, turbidity and light changing. Turbidity is defined as cloudiness in a liquid caused by the presence of suspended particles that scatter and absorb light. Since underwater battery recharging are supposed as a first step to realize a full autonomous/intelligent robot, the deep-sea docking experiments cannot avoid turbidity and low light environment. In previous studies, we had conducted sea docking experiments using a passive (not lighting) marker and image-evaluation function based on only hue information, limiting its operational environment in lower turbid sea with sunshine. Whereas in this study, to improve our system removing above defects, we newly designed an active - light emitting - 3D marker and a fitness function determined by HSV color components to improve the performance of the system especially in a more turbid environment. The advantage of using an active 3D marker and HSV-evaluated function is to be thought as being tolerable and seeable despite clipped whites and scattered light on the camera images caused by turbidity. Additionally, we conducted the docking experiments to verify the robustness of the proposed approach against turbidity and compared recognition results between the previous method and the improved method.**

***Index Terms*—sea docking, turbid environment, stereo vision, underwater vehicle**

I. Introduction

Nowadays, autonomous underwater vehicles (AUVs) are essential in applications such as inspection of underwater structures (e.g., dams and bridges) and underwater cable tracking [1]. Underwater battery recharging through Docking operation is one of the solutions to extend the persistence time of an underwater operation of AUVs. There are many studies on underwater docking [2]- [5]. However, a number of challenging issues hinder these applications, which require high accuracy and robustness against disturbances that occur in the underwater environment. To achieve these tasks in underwater vehicles, we have developed a vision-based docking system using stereo vision.

In an underwater vehicle with a lighting unit installed on it, especially, dynamic lighting environment addresses challenges when the own lighting system is dominant in a deep sea or during a night operation. Additionally, when an underwater vehicle approaches the sea bottom, water turbidity comes in picture as disturbance to be considered and solved for visual servoing. According to the authors' knowledge, there are few studies on the 3D pose estimation under turbidity for underwater vehicles.

In previous works [6]- [8], different experiments to confirm the robustness of our vision-based system using two cameras and a known 3D marker were conducted. Sea trial docking using an ROV as a test bed was conducted in a real sea near Wakayama city in Japan successfully [10]. In previous studies, we had conducted sea docking experiments using a passive (not lighting) marker and image-evaluation function based on only hue information, limiting its operational environment in lower turbid sea with sunshine. To overcome this limitation, in this study, we newly designed an active 3D marker and developed fitness function that is used for real time pose estimation using HSV information to improve the performance of the system especially in turbid and low illumination environment. We conducted the docking experiments to verify the robustness of the proposed approach against turbidity and compared recognition results between the previous method and the improved method.

The remainder of the paper is organized as follows: Section II describes 3D recognition and control. Section III describes

978-1-5386-1654-3/18/$31.00 ©2018 IEEE

the proposed method. Docking experiment against dark and turbid environment for comparing the new method with the previous method in real sea environment is described in section IV. The final section concludes the paper.

II. 3D Move on Sensing (3D-MoS)

A robotic system, named 3D Move-on Sensing (3D-MoS) in which 3D perception enabled by dual-eyes visual pose tracking by using known 3D marker is used in this study for controlling the underwater vehicle's relative pose to the desired one. The 3D-MoS system recognizes a relative pose between a robotic system (remotely operated vehicle (ROV) in this study) and a target object by utilizing 3D model-based recognition using dual-eye camera images with a video frame rate of 30 (fps). In the proposed approach, visual information is directly used in feedback control in real-time. Additionally, developed optimization method named Real-time Multi-step GA (hereafter, RM-GA) is implemented in accordance with the concept of optimization of dynamic images for real-time target tracking.

A. 3D Model-based pose estimation method

Real-time 3D pose estimation using RM-GA was proposed and introduced in previous work [9]. The explanation of RM-GA is briefly described in this section for reader's background. Knowing the information of the target and predefined relative pose to the ROV, the solid model of the target is predefined and projected to 2D images. Comparing the projected solid model image with the captured 2D images by dual cameras, the relative pose difference can be calculated.

In the proposed system, we first create a shape and color attribute of a model based on known 3D target. Then we define a fitness function that represents the correlation between multiple models projected onto images of dual eyes and actual targets appearing in an image of dual eyes. It is possible to set the model shape, light environment or correlation function to take the maximum fitness value when the position and orientation of the 3D model overlaps those of the target. In such a state, the problem of finding the 3D position and orientation of the target is converted to an optimization problem for finding a variable that maximizes the correlation function. Furthermore, by conducting an optimal solution search using the correlation function, it is possible to effectively search for the optimal solution even when the distribution of the correlation function with respect to the position and orientation becomes dynamic multi peak function that will be provided by actual sea environment. The combination of designed 3D target (we called lighting 3D marker in this study) and developed fitness function for dark and turbid environment is the main novelty of this study.

B. RM-GA with fitness function

In this method, the genes which represent the different relative poses of 3D model to the ROV are initiated randomly. Fitness value which is correlation function of projected model against the real target in the image is used as the evaluation

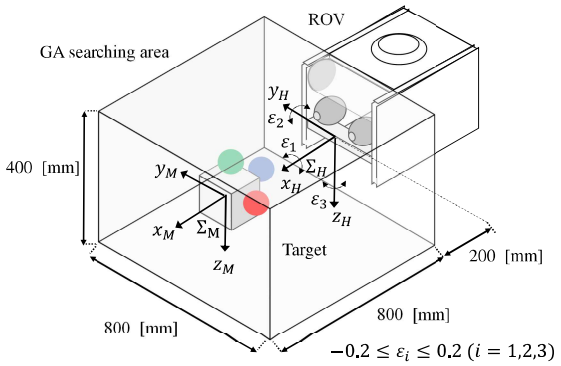

Fig. 1. GA searching area and coordinate systems of the robot and the real target.

parameter of recognition process. According to defined fitness function, the gene with the highest fitness function value represents the pose of the real target. Therefore, the searching problem of real target pose addresses the optimization problem. Even through there are classical computer vision algorithms to obtain the relative pose estimation, GA provides recognition performance in terms of effectiveness, simplicity and repeatable evaluation for real-time performance. Therefore, GA named as RM-GA (Detail explanation can be seen in [11] [12] [13]) in this experimental system is capable of real-time recognition of the moving image effectively and confirmed in our previous works [14] [15]. Through the steps of GA (Selection, Cross over and Mutation), a number of genes that represent different poses are evaluated by the defined fitness function to get the best gene with the most truthful estimated pose. This 3D model-based matching process is executed within 33 (ms) synchronizing with the video rate of dual-eyes camera. Fig. 1 shows searching area of RM-GA. How the fitness function is calculated is explained in section III.

C. Underwater robot system

Remotely controlled underwater robot used in this experiment (manufactured by KOWA) is shown in Fig. 2.

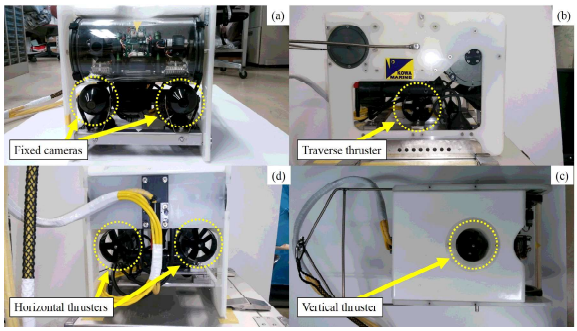

Fig. 2. Underwater vehicle which we used in the experiment.

As the main sensor that is visual sensor for this robot , the two fixed forward cameras are used for 3D object recognition

in visual servo. In the thruster system of ROV, 2 horizontal thrusters with maximum thrust of 9.8 (N), 1 vertical thruster with maximum thrust of 4.9 (N) and 1 lateral thruster with 4.9 (N) are installed.

III. PROPOSED METHOD

To improve the performance of the system against turbid and low illumination environment, we newly designed lighting 3D marker and fitness function (we named it Union fitness function) using HSV information. In the section, a lighting 3D marker and developed fitness function is explained in details.

A. Lighting 3D Marker

We call the target object used in this study "3D marker". A conventional 3D marker did not emit light (passive); thus, in recognition under dark and turbid environments, the robot had to use the lighting mounted on itself. However, in that case, as shown in Fig. 3(A), it has been confirmed that the recognition has failed because the camera image is entirely blurred white. This is thought to be caused by diffused reflection of light on the particles in the turbid water. This is a factor that makes recognition in the dark and turbid environment difficult, which can be a fatal obstacle to use the system in the actual sea area. From this point of view, it can be said that it is necessary to minimize the amount of light reaching the camera in order to prevent diffused reflection and accurately recognize the target. Therefore, we newly propose "lighting 3D marker" which emits light. By doing so, it can take in only the light necessary for recognition, even in higher turbid environment (Fig. 3(B)).

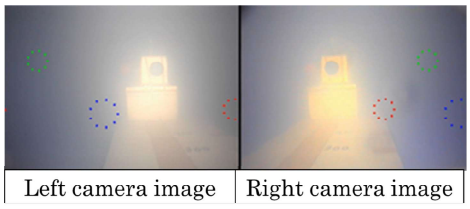

(A) Non-lighting marker in 15.3 FTU

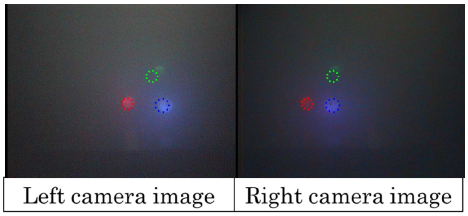

(B) Lighting marker in 18.3 FTU

Fig. 3. Comparison of appearances of a lighting marker and a non-lighting one under dark and turbid environment.

B. Union fitness function using HSV color information

The previous evaluation method used in [7], [9] was based only on the hue value of the target. However, using this method, its relative pose cannot be recognized well while using the lighting 3D marker proposed this time in a dark and turbid environment. The reason is that as the robot approaches the marker, the amount of light reaching the cameras increases, and on the camera image, the strongly emitting part appears white. When using only hue information for evaluation, there is a disadvantage that achromatic colors such as white or black cannot be evaluated correctly. Fig. 4(B) shows the hues distribution of Fig. 4(A). These hues are predefined in Equation 2. In order to achieve accurate recognition, it is necessary that the area of the spheres on the original images is equal to the colored areas on the hue distribution in terms of size. However, the distribution of (B) shows that the defined hue areas are wider than the sphere areas on the original images. This is thought to be caused by light being diffused by particles suspended in water. Although edge detection is performed for estimating a pose of the 3D marker, in this case, edge detection does not work well, thus accurate recognition cannot be performed. On the other hand, compared with (B), it can be seen that the edge of the sphere on 3D marker is clearer in Fig. 4(C). The distribution in (C) is values. Therefore, edge detection based on value is more effective than based on hue under such an environment. Another method newly proposed in the paper is a composite type object evaluation method using three color components of HSV. This is in consideration of the evaluation of "lighting" in addition to the conventional evaluation using "color." As shown in Fig. 5, score is evaluated for each point (pair of points in the case of lighting evaluation) by using correlation function (Eq. (1), (2) and (3)). Then, by synthesizing the two fitness values according to Eq. (4), "union fitness value ($F_{union}(\boldsymbol{\phi}_M^j)$)" which we newly defined is obtained. And finally, $F_{union}(\boldsymbol{\phi}_M^j)$ is calculated for the left and right camera images and determine $F(\boldsymbol{\phi}_M^j)$ by taking the average of them (Eq. (5)). Eq. (4) plays the role of so-called "OR" in which the union fitness value becomes higher if either of the two fitness values (fitness values of color evaluation ($F_{hsv}(\boldsymbol{\phi}_M^j)$) and light emission evaluation ($F_{v_d}(\boldsymbol{\phi}_M^j)$)) is higher. Therefore, the model of the target has redundancy. Here, it is assumed that N_{pairs} has the same value as N_{out} in Eq. (4).

$$p_{v_d}({}^I\boldsymbol{r}_{in}^{(m)}, {}^I\boldsymbol{r}_{out}^{(m)}) = \begin{cases} 1 & (|V({}^I\boldsymbol{r}_{in}^{(m)}) - V({}^I\boldsymbol{r}_{out}^{(m)})| \geq 10) \\ -1 & (otherwise) \end{cases} \quad (1)$$

$$p_{hsv}({}^I\boldsymbol{r}_{in}^{(n)}) = \begin{cases} 1 & \{H_u({}^I\boldsymbol{r}^{(n)}) \in [h_u - 40, h_u + 40] (u = R, G, B), \\ & S({}^I\boldsymbol{r}^{(n)}) \geq 0.10, V({}^I\boldsymbol{r}^{(n)}) \geq 30\} \\ -1 & (otherwise) \end{cases} \quad (2)$$

$$p_{hsv}({}^I\boldsymbol{r}_{out}^{(n)}) = \begin{cases} -1 & \{H_u({}^I\boldsymbol{r}^{(n)}) \in [h_u - 40, h_u + 40] (u = R, G, B), \\ & S({}^I\boldsymbol{r}^{(n)}) \geq 0.10, V({}^I\boldsymbol{r}^{(n)}) \geq 30\} \\ 1 & (otherwise) \end{cases} \quad (3)$$

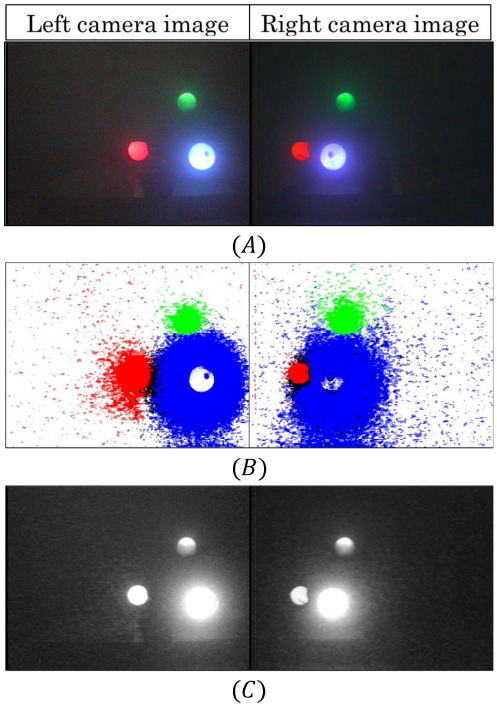

Fig. 4. Original camera images and distributions of each color component in the images. (A) is original images from dual-eye camera. (B) is a distribution of hues extracted from (A). The colored area shows the hue defined for each color and the black and white area shows other hues in (B). (C) is a distribution of values extracted from (A).

$$
\begin{aligned}
F_{union}(\boldsymbol{\phi}_M^j) &= F_{vd}(\boldsymbol{\phi}_M^j) + F_{hsv}(\boldsymbol{\phi}_M^j) - F_{vd}(\boldsymbol{\phi}_M^j) \cdot F_{hsv}(\boldsymbol{\phi}_M^j) \\
&= \frac{\sum_m^{N_{pairs}} p_{vd}({}^I\boldsymbol{r}^{(m)})}{N_{pairs}} + \frac{\sum_n^{N_{in}+N_{out}} p_{hsv}({}^I\boldsymbol{r}^{(n)})}{N_{in}+N_{out}} \\
&\quad - \frac{\sum_m^{N_{pairs}} p_{vd}({}^I\boldsymbol{r}^{(m)})}{N_{pairs}} \cdot \frac{\sum_n^{N_{in}+N_{out}} p_{hsv}({}^I\boldsymbol{r}^{(n)})}{N_{in}+N_{out}}
\end{aligned} \tag{4}
$$

$$
F(\boldsymbol{\phi}_M^j) = \frac{1}{2}({}^L F_{union}(\boldsymbol{\phi}_M^j) + {}^R F_{union}(\boldsymbol{\phi}_M^j)) \tag{5}
$$

The fitness function was designed as an evaluation parameter in the pose estimation process. It is a defined correlation between a projected model and a real target in the image. In Fig. 6, the three solid circles and the three circles outlined with dotted lines represent the spheres on the real target and those on the j-th model obtained from 3D-to-2D projection, respectively. The pose $\boldsymbol{\phi}_M^j$ of the 3D model is an unknown variable composed of six parameters $(x, y, z, \varepsilon_1, \varepsilon_2, \varepsilon_3)$ and is determined in the pose estimation process. The 2D projection of each sphere in the model is divided into two regions, as shown by the dashed circles in Fig. 5. Instead of evaluating the positions of all of the points in the model, only select points are considered, as shown in Fig. 5. When the j-th model is projected onto the 2D images of the left and right cameras, the fitness value for that model is calculated. Portions of the target object that lie inside the inner ($S_{in}(\boldsymbol{\phi}_M^j)$) and outer ($S_{out}(\boldsymbol{\phi}_M^j)$) regions of each corresponding sphere of the projected model proportionally increase and decrease the fitness value, respectively. In addition, ${}^I\boldsymbol{r}_{in}$ and ${}^I\boldsymbol{r}_{out}$ are position vectors of the points on the image existing in $S_{in}(\boldsymbol{\phi}_M^j)$ and $S_{out}(\boldsymbol{\phi}_M^j)$, respectively. Therefore, the fitness function is maximized when the pose of the model fits that of the target object depicted in the images of the left and right cameras. The evaluation parameters of the fitness function were designed to reduce the effect of noise, which is considered here as peaks in the fitness function that represent incorrect poses of the target. The concept of the fitness function in this study can be said to be extension of the work in [17], in which different models, including a model with rectangular surface strips, were evaluated using images from a single camera.

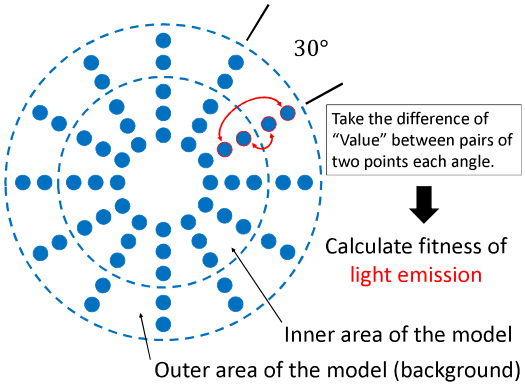

Fig. 5. Projection of the blue sphere of a model with selected sample points. There are a total of 60 points (36(=$N_{in}/3$) and 24(=$N_{out}/3$) points in the inner and outer regions, respectively) in the projection, and the diameter of the inner region is same as that of the actual sphere.

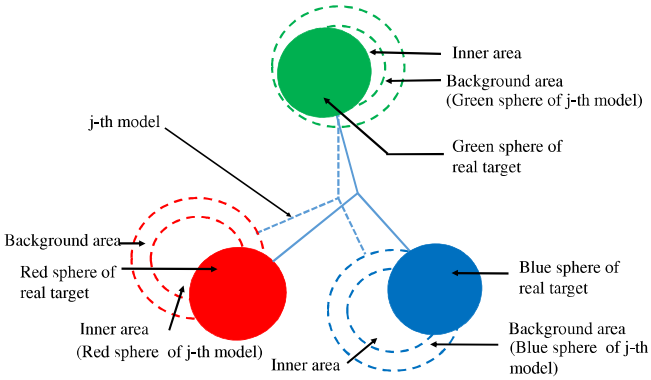

Fig. 6. Real target (solid circles) and projected 3D model (circles with dashed outlines) in a 2D image obtained by the right camera.

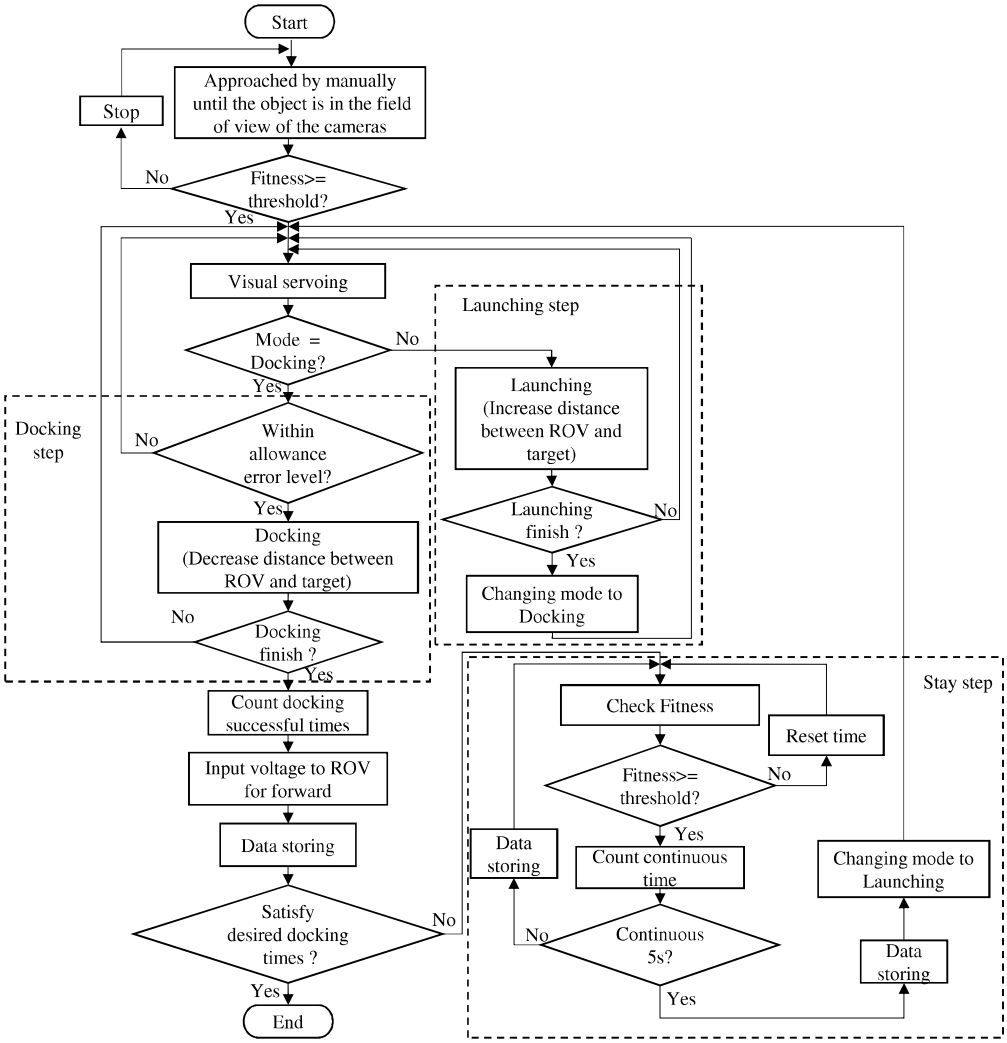

Fig. 7. Flowchart of the docking experiments.

IV. Docking Experiment in the Sea with Turbid Environment

A. Outline of the experiment

Using the system proposed in this study, we conducted docking experiments in real sea areas in a turbid and dark environment assuming sea floor with turbid water. The sea we conducted the experiments is Seto-naikai in Japan, and the turbidity increases due to the influence such as the proliferation of plankton from summer to autumn [18]. This experiment was conducted after sunset on September 28, 2017. The turbidity of this sea is highest in September in the year. The experiment was conducted to ascertain whether docking can be performed imitating power supply operation and the target recognition in such an environment. For comparison, the same experiment was also conducted using object evaluation method utilizing only hue information. These experiments were conducted between 6:59 pm and 7:29 pm during which the turbidity of the seawater was 13.8 (FTU) to 15.0 (FTU). FTU is an abbreviation for "Formazin Turbidity Unit", which is a type of unit that expresses turbidity. Turbidity of seawater was measured using a turbidity sensor (model: TD-500 manufactured by OPTEX).

B. Strategy of Docking Operation

In this subsection, the design of the docking procedure as shown in Fig. 7 is discussed with the detailed flowchart. The sea docking strategy is same as the pool test except for the approaching step and stay step. To perform the continuously repeated docking experiments, the proposed docking system includes five steps: (1) Approaching step (approached the docking station by manually until the 3D marker is in the field

of view of the cameras), (2) visual servoing step (initial state of the docking), (3) docking step (fitting the docking pole into the docking hole), (4) stay step (staying in front of the docking station for data storing without performing visual servoing), and (5) launching step (go back to the desired position). At the start of the docking procedure, the ROV approached the docking station by manually until the 3D marker is in the field of view of the cameras which are mounted in front of the ROV. After detecting the 3D marker, the fitness value recognized by RM-GA was compared with the control threshold of fitness value. If the recognized fitness value is lower than the control fitness value which means that the ROV could not detect the 3D marker, the ROV approached the docking station by manually again. If the recognized fitness value is higher than the control fitness value, the proposed system switched from manual to automatic control of the visual servoing state.

In the visual servoing step, the ROV estimated the relative pose of the vehicle with respect to the 3D marker. In this state of visual servoing, the distance between the ROV and the 3D marker was about 600 (mm). After visual servoing step is satisfied, docking step and launching step are performed as shown in Fig. 7. If the ROV is stable within the allowance error range that is defined experimentally, it switched from the visual servoing step to the docking step. In the docking step, the ROV is stable for docking within the allowance error ranges. In this step, the ROV automatically goes forward to insert the docking pole into the docking hole by decreasing the distance between the vehicle and the target. The docking step was completed with the distance 350 (mm) between the ROV and the 3D marker. After finished staying for the completion of docking, the successful docking time was counted. After counting the docking time, the two docking poles are propelled to the wall of the rectangle docking hole by applying the constant input voltage to ROV thrusters for staying in front of the docking station. And then, the GA-PC stores the data log in files from memory into the hard disk for further analysis and the desired docking times were checked. If the desired docking times are satisfied, the continuously repeated docking experiment is finished. If the desired docking times are not satisfied, the stay step is performed.

In the staying step, the fitness value recognized by RM-GA of the current condition is checked and this fitness value is compared with the control threshold fitness value. If the current fitness value is larger than the control fitness value, the time is started count continuously. If the current fitness value is lower than the control fitness value, time is reset to zero and the fitness value is checked again. The time for staying in front of the docking station took about 5 (s). The data storing is performing during 5 (s) counting. After finished staying for 5 (s), the final data is stored log in files from memory into the hard disk. After storing the data, the operation changed to the launching mode.

In the launching step, the ROV goes back to the desired position by increasing the distance between the ROV and the 3D marker. When the ROV reached the desired position about 600 (mm), the launching step finished. After finishing the launching step, the docking step was performed again. However, if the launching process no longer meet the conditions of desired position, it returns to the visual servoing step.

C. Experimental Results and Consideration

Figure 8 shows the results of docking experiments when using the conventional target evaluation methods, and Fig. 9 shows the results of docking experiments when using the target evaluation method proposed in this study. Since the fitness of Fig. 8(A) is not normalized, the maximum value is $1.\dot{6}$. The docking operation is realized by decreasing the target value in the x-axis direction when the recognition values of y, z and ε_3 all are located within "Error allowance." By performing visual servoing from Fig. 8(A)-(D), it can be seen that the ROV could not be controlled to be stable for docking. Consequently, docking could not be done. It is considered that the main reason for this is that the amplitude of the recognition value of ε_3 is too large and often not located within "Error allowance". Regarding ε_1 and ε_2, pitching and rolling are neglected in controlling the ROV due to their self-stability. Figure 8(E) shows the camera image about 104 (s) after starting the experiment and a model of the target object drawn with dotted circles generated on the images according to the recognition value $\boldsymbol{\phi}_M^1 = (x, y, z, \varepsilon_1, \varepsilon_2, \varepsilon_3)$ at that time. From this figure, it can be seen that the model does not coincide with the target on the image and accurate recognition is not performed.

On the other hand, in the docking experiment using the target evaluation method proposed in this paper in Fig. 9, the recognition value in the x-axis direction decreases more smoothly, so that the docking can be performed. The recognition values of y and z are not greatly different from those when using conventional ones, but it can be seen that the recognized values for the orientation of the target are greatly different, and the fluctuation of the values is suppressed. Even with the camera image of about 50 (s) after the start of the experiment and the model at that time (Fig. 9(E)), the target object and the model are approximately coincident and it means that accurate recognition is possible. According to experimental results in Fig. 8, Fig. 9, it can be concluded that newly designed active marker and developed fitness function are effective for sea docking in turbid and low illumination environment overcoming the limitation of the previous work.

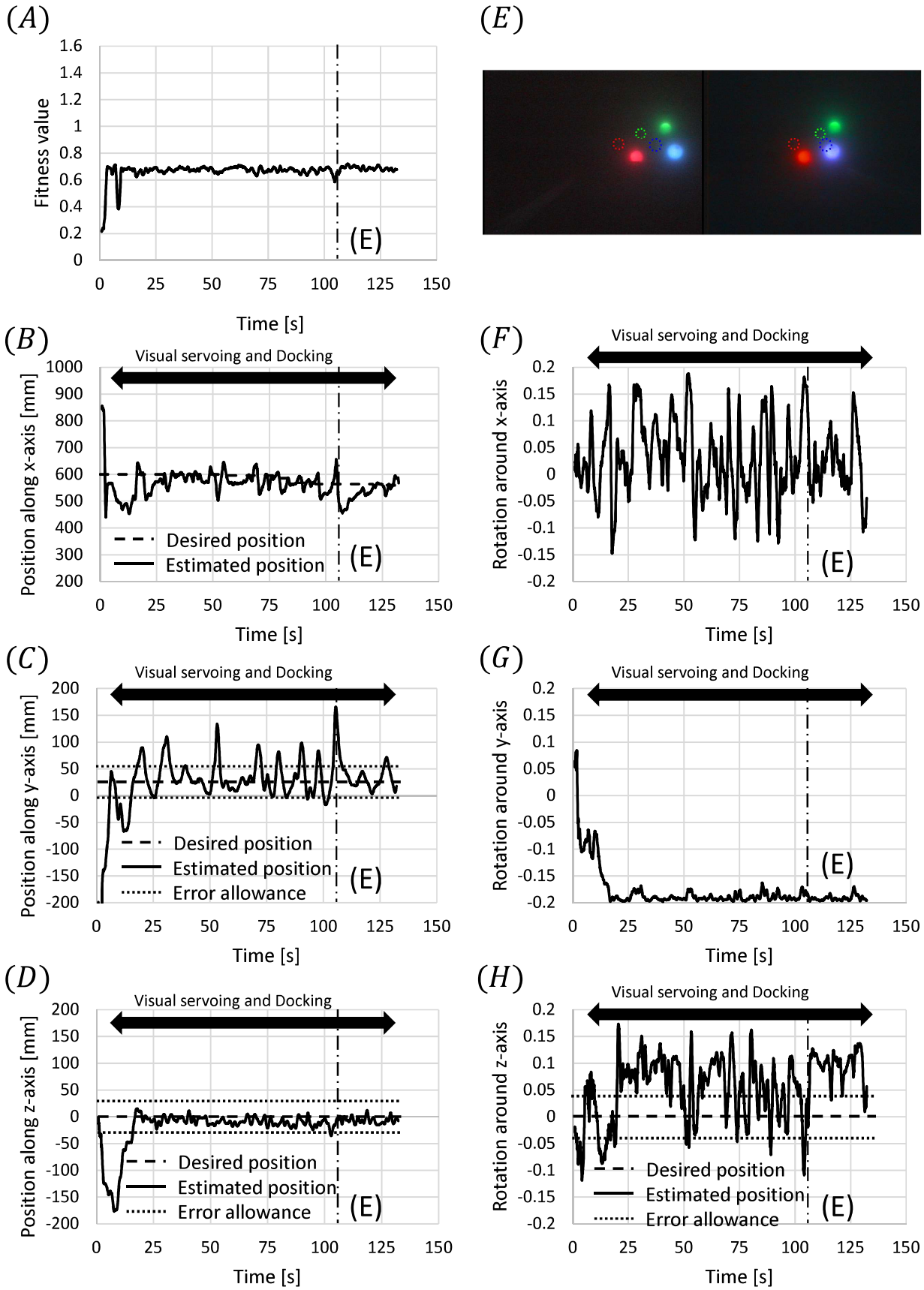

Fig. 8. Results of continuous iterative docking experiment using fitness function based on only hue. (A)Fitness value, (B)Position along x-axis, (C)Position along y-axis, (D)Position along z-axis, (E)Camera images and models in about 104(s), (F)Rotation around x-axis, (G)Rotation around y-axis,and (H)Rotation around z-axis. Note that rotation around x-, y-, and z-axis are in quaternion.

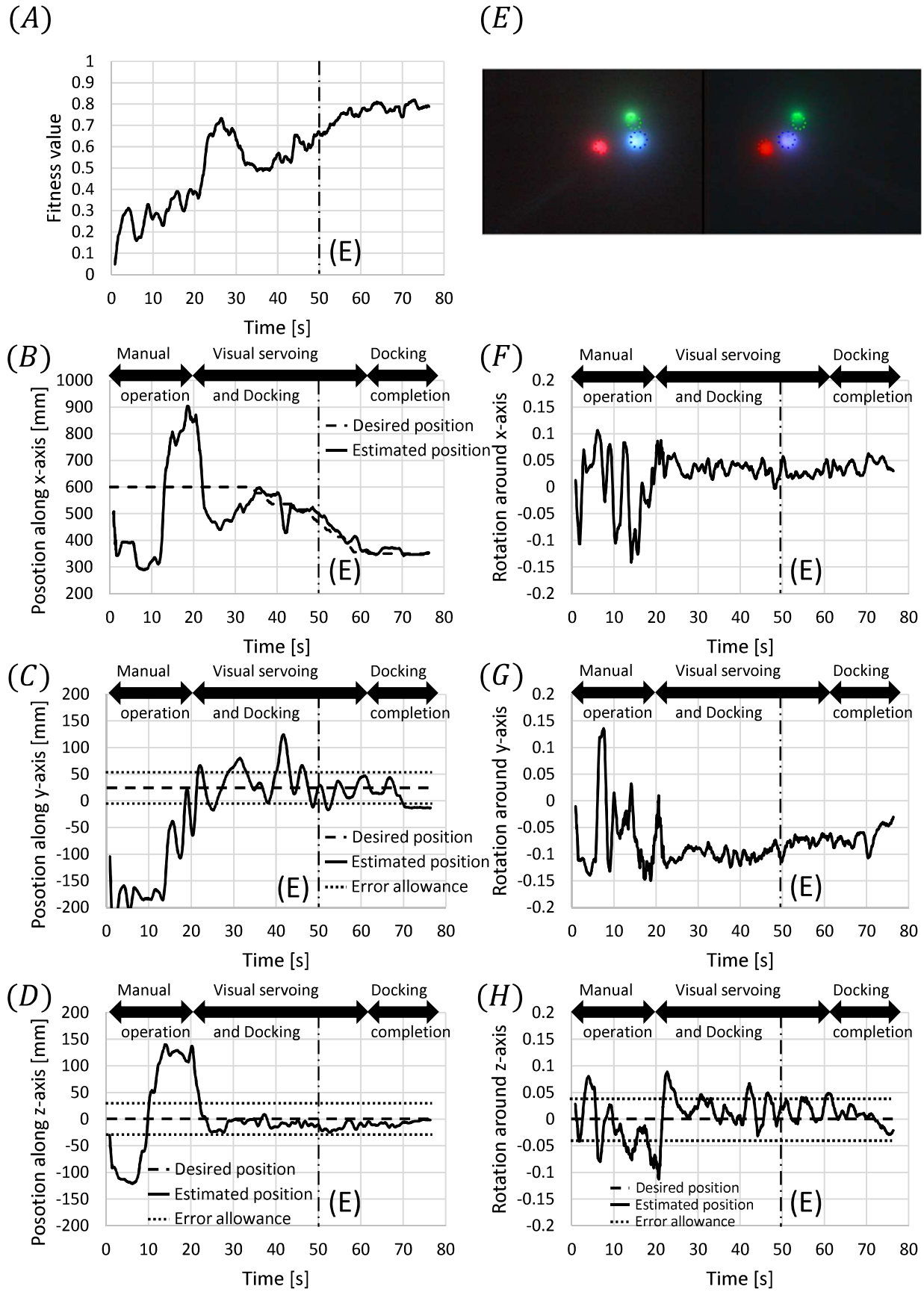

Fig. 9. Results of continuous iterative docking experiment using fitness function based on HSV; (A)Fitness value, (B)Position along x-axis, (C)Position along y-axis, (D)Position along z-axis, (E)Camera images and models in about 50(s), (F)Rotation around x-axis, (G)Rotation around y-axis,and (H)Rotation around z-axis. Note that rotation around x-, y-, and z-axis are in quaternion.

V. Conclusion

In this paper, we proposed new method on the measurement of the position and orientation of the target under the dark and turbid environment and conducted docking experiments to compare the conventional method with new one at a real sea area with turbid water in Japan and demonstrate its utility. It was able to realize recognition and docking operation in turbid water (15.0 (FTU)). We conducted a docking operation from 600 (mm) distance between the robot and the target in this study. By improving the system, the operation from farer distance over 600 (mm) under dark and turbid environment will be conducted in the future work.

VI. Acknowledgment

The authors would like to thank Ministry of Education, Culture, Sports, Science and Technology, Mitsui Engineering and Shipbuilding Co. Ltd. and Kowa Corporation for their collaboration and support for this study.

References

[1] B.A.A.P. Balasuriya, M. Takai, W.C. Lam, Tamaki Ura and Y. Kuroda: "Vision based Autonomous Underwater Vehicle Navigation: Underwater Cable Tracking," Proc. MTS/IEEE OCEANS Conf., vol.2, pp.1418-1424, 1997.

[2] Robert S. McEwen, Brett W. Hobson, Lance McBride and James G. Bellingham: "Docking Control System for a 54-cm-Diameter (21-in) AUV," IEEE Journal of Oceanic Engineering, Vol. 33, NO. 4,pp. 550-562, October 2008.

[3] Ken Teo, Benjamin Goh and Oh Kwee Chai: "Fuzzy Docking Guidance Using Augmented Navigation System on an AUV," IEEE Journal of Oceans Engineering, Vol. 37, NO. 2, April 2015.

[4] Narc s Palomeras, Antonio Pe nalver, Miquel Massot-Campos, Guillem Vallicrosa, Pep Llu s Negre, J. Javier Fernndez, Pere Ridao, Pedro J. Sanz, Gabriel Oliver-Codina and Albert Palomer: "I-AUV docking and intervention in a subsea panel," IEEE/RSJ International Conference on Intelligent Robots and Systems, Chicago, IL, pp 2279-2285, 2014.

[5] J.-Y. Park, B.-H. Jun, P.-M. Lee and J. Oh: "Experiments on vision guided docking of an autonomous underwater vehicle using one camera," Ocean Eng., Vol. 36, No. 1, pp. 48-61, Jan. 2009.

[6] Myo Myint, Kenta YONEMORI, Akira YANOU, Shintaro ISHIYAMA and Mamoru MINAMI,: "Robustness of Visual-Servo against Air Bubble Disturbance of Underwater Vehicle System Using Three- Dimensional Marker and Dual-Eye Cameras," Proceedings of the International Conference OCEANS15 MTS/IEEE, Washington DC, USA, pp.1-8, 2015.

[7] Myo Myint, Kenta Yonemori, Akira Yanou, Mamoru Minami and Shintaro Ishiyama,: "Visual-servo-based Autonomous Docking System for Underwater Vehicle Using Dual-eyes Camera 3D-Pose Tracking," Proceedings of the 2015 IEEE/SICE International Symposium on System Integration, Nagoya, Japan, pp.989-994, 2015.

[8] Myo Myint, Kenta YONEMORI, Akira YANOU, Khin Nwe Lwin, Mamoru MINAMI and Shintaro ISHIYAMA: "Visual-based Deep Sea Docking Simulation of Underwater Vehicle Using Dual-eyes Cameras with Lighting Adaptation," Proceedings of the International Conference OCEANS16 MTS/IEEE, Shanghai, China, pp.1-8, 2016.

[9] Myo Myint, Kenta Yonemori, Khin Nwe Lwin, Akira Yanou, Mamoru Minami: "Dual-eyes Vision-based Docking System for Autonomous Underwater Vehicle: An approach and Experiments" J Intell Robot Syst (2017). DOI 10.1007/s10846-017-0703-6.

[10] Myo Myint, Kenta YONEMORI, Akira YANOU, Khin Nwe Lwin, Naoki Mukada and Mamoru MINAMI: "Dual eyes visual based sea docking for sea bottom battery recharging," Proceedings of the International Conference OCEANS16 MTS/IEEE, Monterey, USA, pp.1-7, 2016.

[11] Song W., Minami M. and Aoyagi S.: "Feedforward On-line Pose Evolutionary Recognition Based on Quaternion", *Journal of the Robot Society of Japan*, Vol.28, No.1, pp.55-64 (in Japanese), 2010.

[12] Song W. and Minami M.: "3-D Visual Servoing Using Feedforward Evolutionary Recognition", *Journal of the Robot Society of Japan* , Vol.28, No.5, pp.591-598 (in Japanese), 2010.

[13] Wei. Song, M. Minami, Fujia Yu, Yanan Zhang and Akira Yanou: "3-D Hand and Eye-Vergence Approaching Visual Servoing with Lyapunouv-Stable Pose Tracking", *IEEE Int. Conf. on Robotics and Automation (ICRA)*, pp. 5210-5217, 2011.

[14] Yu F., Minami M., Song W., Zhu J. and Yanou A.: "On-line Head Pose Estimation with Binocular Hand-eye Robot based on Evolutionary Model-based Matching", *Journal of Computer and Information Technology*, Vol.2, No.1, pp.43-54, 2012.

[15] Suzuki H. and Minami M.: "Visual Servoing to catch fish Using Global/local GA Search", *IEEE/ASME Transactions on Mechatronics*, Vol.10, Issue 3, pp.352-357, 2005.

[16] Hutchinson, S., Hager, G.D. and Corke, P.I.: "A tutorial on visual servo control, IEEE transactions on robotics and automation", 12(5), pp.651-670, 1996.

[17] Song W, Minami M, Aoyagi S: "On-line stable evolutionary recognition based on unit quaternion representation by motion-feedforward compensation", International Journal of Intelligent Computing in Medical Sciences & Image Processing, 2(2), pp.127-139, 2008.

[18] Shin-ichi Uye, Hiroshi Kuwata, Takuo Endo: "Standing Stocks and Production Rates of Phytoplankton and Planktonic Copepods in the Inland Sea of Japan", Journal of the Oceanographical Society of Japan, Vol. 42, pp. 421-434, 1987.